Tunable WDM sampling pulse streams using a spatial phase modulator in a biased pulse shaper

David Sinefeld,* Dror Shayovitz, Ori Golani, and Dan M. Marom

Applied Physics Department, Hebrew University, Jerusalem 91904, Israel

**Corresponding author: sinefeld@gmail.com*

Received September 12, 2013; revised December 11, 2013; accepted December 21, 2013; posted December 23, 2013 (Doc. ID 197463); published January 29, 2014

We generate transform-limited WDM optical sampling pulse bursts by filtering ultrashort pulses from a mode-locked laser. A phase spatial light modulator (SLM) is used in a biased pulse shaper to circumvent the need to modulate with 2π phase wraps, which are known to limit the phase response. The arrangement compresses and retimes user-selectable bandwidths from the optical short pulse source with precise control of pulse bandwidth, pulse stream rates, and duty cycle. © 2014 Optical Society of America

OCIS codes: (130.7408) Wavelength filtering devices; (320.5540) Pulse shaping.
http://dx.doi.org/10.1364/OL.39.000642

Photonic analogs to digital converters (ADC) have attracted interest for the past four decades, due to their potential for high sampling speed and accuracy [1,2]. Many photonic ADC implementations are based on optical sampling, with short pulses generated from a mode-locked laser (MLL), due to their extremely low jitter characteristic, for implementing an optical sample and hold function [3]. An additional reduction in ADC rate may be provided by WDM sampling, effectively slowing down the optoelectronic detection speed by the wavelength parallelism factor [4]. One way to achieve this is by chirping the optical pulses, resulting in the instantaneous frequency varying linearly with time as the stretched pulse traverses the optical modulator being fed by the analog voltage signal, and subsequent slower detection after further dispersion [5] or wavelength demultiplexing [6]. Similar concepts are used with parametric processing to a frequency mapped signal, performing temporal imaging, and serial-to-parallel conversion [7,8]. However, a linear chirp is not the desired sampling format; a WDM pulse sampling sequence is desired, where each pulse is transform limited and distinguished by wavelength. Generation of WDM pulse streams using continuous wave (CW) sources and an active electro-optic modulator (EOM) have been demonstrated [9,10], as well as by intracavity modulation [11–13] or by active modulation of a MLL output [14,15]. All the above schemes are limited by the EOM bandwidth (BW) limits, leaving them susceptible to timing jitter from the driving electronics. These limitations can be overcome by using an MLL source and passive optical filtering. This approach for WDM pulse sampling sequence generation have been demonstrated [16,17] by cascading a dispersive medium (fixed or tunable broadband dispersion arrangement) and compensating with a fixed or tunable opposite dispersion with a finite free spectral range (FSR) [18], thus generating a staircase group delay (GD) response. While the tunable arrangement is GD jump adjustable per FSR (thereby setting the sampling rate), its BW is set by the FSR and is reduced for high dispersion settings due to BW narrowing, and its cumulative losses are too high.

Here, we present a new photonic spectral processor (PSP) (Fig. 1) based on a folded bulk-optic arrangement with a reflective, phase-only spatial light modulator (SLM) using liquid crystal on silicon (LCoS) technology. This processor can manipulate the spectral components to generate tunable GD values across arbitrary BW slices of an incident ultrashort pulse. With this processor we demonstrated WDM optical sampling streams at 10, 15, and 20 GHz, when starting with a 2.5 GHz repetition rate source. Other configurations are also possible. This PSP has the advantage of being a completely passive system, as well as not requiring long optical fibers that may incur increased jitter (such as in [12]). Furthermore, it is highly flexible, allowing fine control over pulse amplitude and timing. The PSP design is a modification of the classic 4-f pulse shaper [19–21], as outlined next. The PSP could be implemented as a conventional free-space, 4-f pulse shaper [22,23]. At the Fourier plane, spectral linear phase tilt functions in the dispersion direction would translate to GD, as desired. However, typical LCoS devices, on which we need to set the linear phase functions, have a 2π phase modulation depth limit.

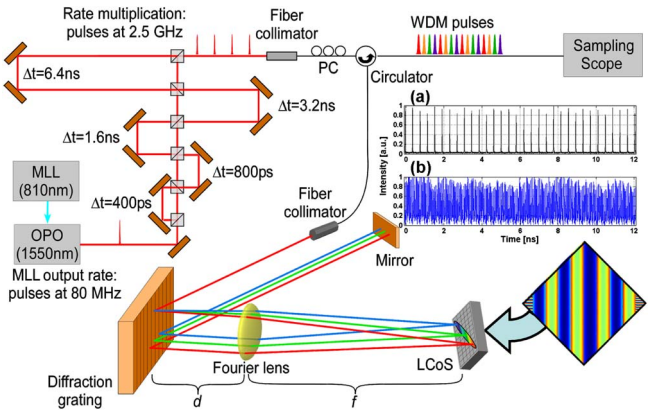

Fig. 1. PSP layout for generating WDM pulse streams and the experimental setup. Ultrashort pulses (100 fs) from an MLL at 80 MHz rep rate are rate increased to 2.56 GHz with five delay arms. The pulses are filtered by the LCoS processor, generating a tunable rate WDM pulse stream. Quadratic phase patterns on the LCoS generates 8×100 GHz WDM pulse stream. Inset: sampling scope measurements of (a) 32 pulses directly after the five delay lines and (b) 32×8 WDM pulse stream measured after the PSP filtering.

Hence, the linear phase is applied modulo 2π, forming a blazed grating. In theory, this would operate identically; in practice, LCoS device performance is limited by finite pixel size and discrete phase levels [24,25]. Moreover, LCoS suffers from fringing fields in the LC layer at the abrupt $2\pi \to 0$ phase transition, which smoothen the sharp edges of the phase blazed grating. As the encoded tilt angle is increased and the blazing period is decreased, the fringing field distortion occupies a larger fraction of the blazing period and the phase accuracy and device performance deteriorate rapidly [Fig. 2(a)].

Our PSP modifies the classic 4-f pulse shaper setup by displacing the diffraction grating from the lens front focal plane, creating a biased pulse shaper. This Δz displacement generates a spherical phase front at the Fourier plane that translates to a quadratic spectral phase, hence mapping to chromatic dispersion (CD) according to [18,26],

$$\mathrm{CD} = \frac{2\lambda_0}{c_0}\left(\frac{d\theta}{d\lambda}\right)^2 \Delta z, \tag{1}$$

where $d\theta/d\lambda$ is the angular dispersion at the diffraction grating. While the CD giving rise to chirped waveforms is constant, the phase slope grows quadratically. We next apply with the LCoS SLM local, identical, quadratic phase functions on each BW slice, required to compensate locally for the CD. The cumulative effect of the global optical quadratic phase front from the grating displacement with the locally encoded quadratic spatial phase results in a net linear phase function. The resulting linear phase slope grows for BW slices further from the optical axis, but the encoded quadratic phase is the same and is mostly within the LCoS 2π dynamic range. Hence, we do not need to apply the modulo 2π operation and have excellent phase response [Fig. 2(b)]. Moreover, having a controllable LCoS device in the spectral processor allows for additional fine tuning of the filter response. We introduce fine tilts in the dispersion direction to accurately set the pulse timing, in effect compensating for the deviations from linearity of the grating angular dispersion. We further power balance the generated pulse sequence by introducing fine tilts in the axis orthogonal to dispersion, impacting the fiber coupling efficiency. The ability to fine tune the response is limited only by the resolution of the LCoS device.

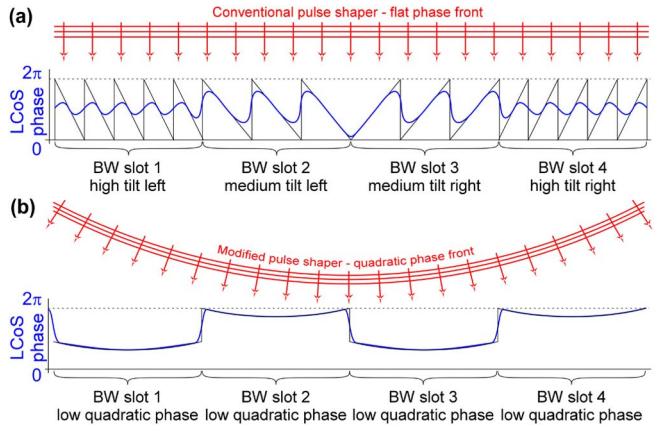

Fig. 2. (a) Interpretation of LCoS phase response (blue, curve) to blazed grating pattern (black, sawtooth), required for retiming in a conventional pulse shaper. (b) LCoS response to low quadratic phase in our modified, biased pulse shaper. Both designs targeted to retime BW slots, but response in (b) outperforms that of (a). Phase offset between adjacent BW slots in (b) is intentionally placed to better carve channels.

To utilize the greatest optical BW using our square LCoS (BNS model P512, 512 pixels × 512 pixels of 15 μm size, 1.55 μm operation), we mount it at 45° and operate along the diagonal, thus obtaining about 10 mm of usable device length. Dispersion is provided by an 1100 gr/mm diffraction grating that is struck not far from Littrow, and we use an $f = 500$ mm lens. The optical processor is further double passed by reflecting the output light back toward the input fiber, and input/output light is separated by an optical circulator. This second pass unravels the space-time coupling effect and doubles the amount of obtainable dispersion. The 500 mm path from lens to LCoS plane was folded for compact realization, resulting in a footprint of 40 cm × 20 cm for the PSP. The diffraction grating was set 180 mm away from the lens ($\Delta z = 320$ mm), yielding CD = 61.7 ps/nm. The relation between the CD and the step height, ΔGD, is given by

$$\Delta\mathrm{GD}\ [\mathrm{ps}] = \mathrm{CD}\ [\mathrm{ps/nm}] \cdot \Delta\lambda\ [\mathrm{nm}], \tag{2}$$

where $\Delta\lambda$ is the curved pulse, BW, determined by the channel width encoded on the SLM (Fig. 1). The duty cycle (d.c.) of the pulse train is set by the ratio between pulse width, τ, and the time separation between pulses ΔGD. For transform limited pulse $\tau = 1/\Delta\nu$, hence,

$$\mathrm{d.c.} = \frac{\tau}{\Delta\mathrm{GD}} = \frac{1/\Delta\nu}{\mathrm{CD}\cdot\Delta\lambda} = \frac{(\lambda/\Delta\lambda)^2}{\mathrm{CD}\cdot c_0}, \tag{3}$$

where $\Delta\nu$ is the optical pulse BW in GHz. The CD value of 61.7 ps/nm was chosen in order to obtain 50 ps GD jumps with 100 GHz (0.81 nm) grid channel spacing, which leads to a 20 GHz sampling pulse sequence and a d.c. of 0.2. Setting the PSP to different CD values (by changing Δz) with the same spectral spacing will result in different d.c. The LCoS aperture enables access to 6.4 nm (800 GHz) of the available optical BW, allowing for the generation of 8 × 100 GHz channels, resulting in 20 GHz WDM optical pulse sampling bursts of 400 ps duration. The processor was characterized with a LUNA Optical Vector Analyzer (OVA), demonstrated 10 dB insertion losses (IL) (including the double passing of the optical circulator), and flat GD within each channel. GD spikes were observed on some channel transitions, but their significance is negligible, since these frequency components are significantly attenuated. The LCoS's phase settings were fine tuned for proper GD jumps between spectral bands (see Fig. 3-left).

We used Spectra Physics Tsunami+Opal MLL, emitting $\lambda = 1.55$ μm, 80 MHz rate, and 100 fs pulses. The pulse rate was increased to 2.56 GHz using five unequal path delay arm interferometers in cascade, resulting in a pulse stream spaced at 400 ps (Fig. 1, inset). The $2^5 = 32$ pulse copies exhibited uneven coupling to a single mode fiber, giving rise to power variations between pulses. This

unwanted result can be overcome easily by using a higher rate MLL.

We used polarization control to adjust the polarized MLL output to the PSP polarization axis. The pulses were filtered by the PSP, with the computer-controlled LCoS SLM. Generated WDM pulse streams were measured with a high-speed optical sampling scope (65 GHz, 1000 averages). The PSP was configured for slicing the 800 GHz optical BW to 8×100 GHz, 6×133 GHz and 4×200 GHz spectral channels, giving rise to WDM pulse rates of 20, 15 and 10 GHz with d.c. values of 0.2, 0.1 and 0.05, respectively. The timing and intensity flatness were tweaked with LCoS phase tilts, to the resolution limit of the sampling scope (Fig. 3-right).

To ascertain that pulses are wavelength distinguishable, we dropped channels with the LCoS (by applying vertical phase tilt along specific channels), and the corresponding wavelength pulses disappeared from each pulse burst (Fig. 4). Two photon absorption-based interferometric intensity autocorrelations using a Si photodetector were performed in order to measure single pulse duration. The results (Fig. 5) were compared to the expected pulse duration according to the spectral response measured for the PSP, obtaining pulses widths of 10.6, 7.5 and 5.7 ps for the 100, 133 and 200 GHz pulse width, respectively (pulse duration values were calculated from the autocorrelation FWHM results which are 1.33 times longer for sinc shaped

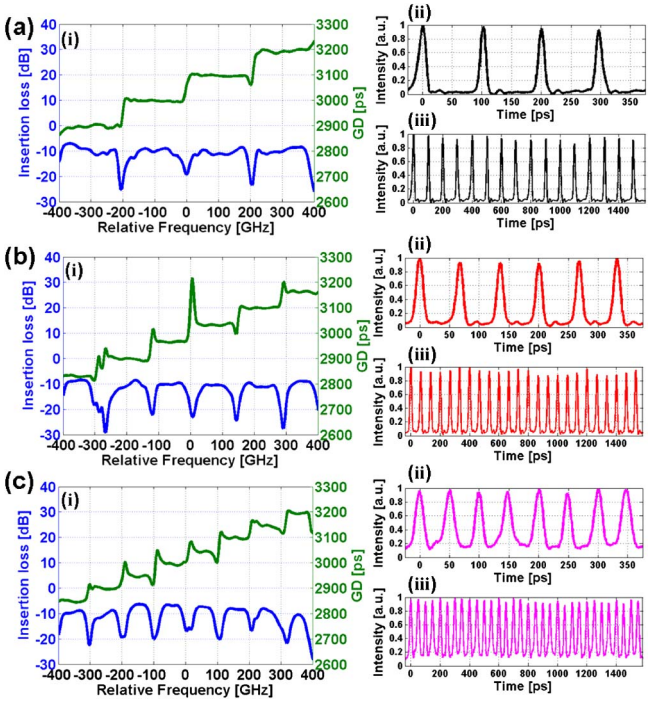

Fig. 3. Experimental results of transform-limited WDM pulse stream generation: (i) PSP group delay and insertion loss measurements from LUNA OVA. Generated pulse streams, measured by sampling scope: (ii) zoom in and (iii) large scale. Three pulse stream rates demonstrated: (a) 4×200 GHZ pulses, for 10 GHz stream rate, and d.c. = 0.05; (b) 6×133 GHz pulses, for 15 GHz stream rate, and d.c. = 0.1; (c) 8×100 GHz pulses, for 20 GHz stream rate, and d.c. = 0.2. The plotted pulse widths are limited by the scope bandwidth (65 GHz) and are actually transform limited, as shown in Fig. 5.

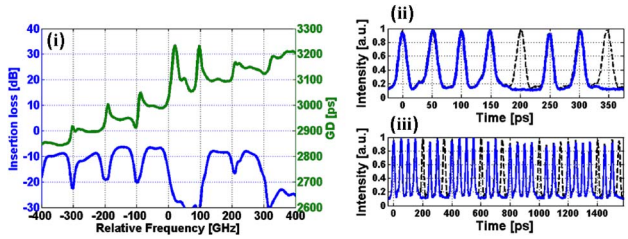

Fig. 4. Demonstration of wavelength distinction of 8×100 GHz WDM pulses within the 20 GHz stream, by attenuating channels 5 and 8 with vertical SLM phase. (i) Spectral transmission and GD. Right—generated pulse stream (blue line): (ii) zoom in and (iii) large scale. Black dashed line shows the pulse stream without channel 5 and 8 attenuation.

pulses), demonstrating that the pulses are indeed transform limited.

In order to measure the timing jitter of the PSP, we used a high speed photodetector connected to a 12 GHz BW real-time scope with a sampling rate of 40 GS/s. With this scope we characterized the temporal jitter of the optical system when configured for the 10 GHz rate pulse stream generation over a time span of 26.2 μs (memory size limited). The measured signal was then sampling rate upconverted by a low pass interpolation algorithm with a linear phase finite impulse response (FIR) filter [27]. This way, we increased the sampling rate by a factor of 250, enabling for fine determination of pulses position [Fig. 6(a)]. We deduce the interpulse jitter within a stream by measuring peak positions of pulses 2–4 with respect to the first pulse, and evaluating the histograms of the 3 temporal delays [Figs. 6(b)–6(d)]. The interpulse delay histograms demonstrate mean values of 0.099, 0.2 and 0.303 ns, which differ a little from the desired 0.1, 0.2 and 0.3 ns delays for 10 GHz sampling because of small errors in the slope that was applied with the SLM. The standard deviation values of the jitter histogram are 0.56, 0.82 and 0.97 ps, respectively. We should emphasize that the interpulse jitter is not random in nature, as the PSP is a passive filtering solution. Timing errors introduced

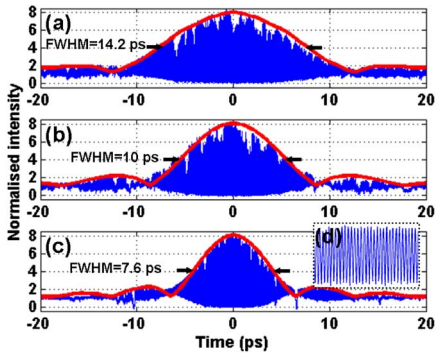

Fig. 5. Intensity autocorrelation (AC) measurement of a single pulse from the pulse stream: (a) 100 GHz pulse BW, (b) 133 GHz pulse BW, and (c) 200 GHz pulse BW. The red line was calculated by applying an FFT on the measured LUNA spectrum, proving that pulses are indeed transform limited (note that the intensity autocorrelation pulse width is 1.33 times longer than the actual pulse duration), and (d) is a zoom in on the intensity autocorrelation fringes pattern.

by the PSP can be considered as deterministic periodic jitter, a well-known phenomenon in the field of time-interleaved ADCs. Some random jitter will be contributed by mechanical/thermal variations in the PSP, but these are very slow compared the sampling rates presented.

In addition to PSP jitter, which only effects the inter pulse jitter, we also measured the MLL source jitter, using the same real time sampling and interpolation method in order to extract exact pulse positions. The results show a jitter of 0.93 ps for the MLL source (Fig. 7).

We note that our high-speed real-time scope (Agilent Infiniium 80000) has a time interval jitter error specification of ~1 ps, which is of the same magnitude of all our jitter measurements. The MLL's jitter is 100 fs (manufacturer specification), asserting that the reported jitter was limited by the measurement and not by the system. Hence, these measurements can serve only as an upper (worst) limit to our system performance and we can confidently assert that the actual PSP jitter is much lower, as the passive filtering solution should not introduce any timing or amplitude jitter, as evidenced in the measured LUNA OVA response (Fig. 3). Therefore, overall random timing jitter originates solely at the laser source. Incorporating the PSP with a low jitter source will therefore provide a low jitter WDM pulse stream.

The system proved stable, accurate, repeatable, and robust, showing the ability to create WDM pulse sampling streams with controllable BW, rate, and duty cycle. The system was easily transferred within the lab, and has the ability to equalize spectral channels with the SLM. Moreover, the optical arrangement can be optimized to support different BW and temporal delays by choices of gratings and lenses under constraint of SLM size.

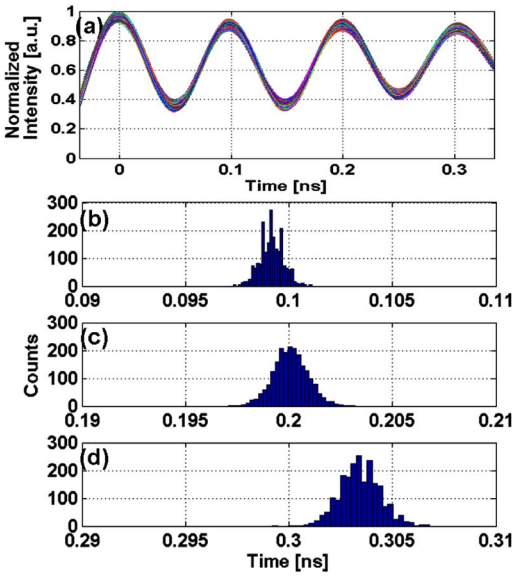

Fig. 6. Real time scope results of 4×200 GHz pulse stream, configured for a 10 GHz stream rate, and d.c. = 0.05 (scope's 12 GHz BW elongates pulse duration). (a) Interpolation of the temporal results showing 0.1 ns difference between pulse positions, where the pulses are timed according to the folding period; (b)–(d) histograms of the interpulses jitter, showing the temporal delay for the 3 pulses when the first pulse serves as a reference. Mean values closely match desired values and standard deviation is less than 1 ps.

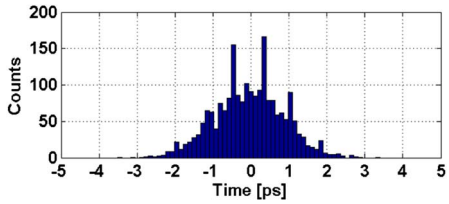

Fig. 7. Jitter histograms of the MLL source. The standard deviation of the histogram is 0.93 ps.

Finally, the system can be utilized as a WDM pulse sampling stream for ultrahigh sampling rate photonic ADC applications when using a faster MLL source (e.g., a 10 GHz repetition rate MLL).

The authors would like to thank the Ministry of Industry Kamin program for funding.

References

1. G. C. Valley, Opt. Express **15**, 1955 (2007).
2. B. L. Shoop, *Photonic Analog-to-Digital Conversion* (Springer, 2000).
3. F. X. Kärtner, J. Kin, J. Chen, and A. Khilo, Frequenz **62**, 171 (2008).
4. J. U. Kang and R. D. Esman, Electron. Lett. **35**, 60 (1999).
5. Y. Han and B. Jalali, J. Lightwave Technol. **21**, 3085 (2003).
6. J. Kim, M. J. Park, M. H. Perrott, and F. X. Kärtner, Opt. Express **16**, 16509 (2008).
7. M. A. Foster, A. C. Turner, R. Salem, M. Lipson, and A. L. Gaeta, Opt. Express **15**, 12949 (2007).
8. H. C. Hansen Mulvad, E. Palushani, H. Hu, H. Ji, M. Galili, A. T. Clausen, M. Pu, K. Yvind, J. M. Hvam, P. Jeppesen, and L. K. Oxenløwe, in *ECOC 2011 PDD* (2011) Th.13.A.2.
9. J. V. Howe, J. Hansryd, and C. Xu, Opt. Lett. **29**, 1470 (2004).
10. X. Fu, H. M. Zhang, Y. Peng, and M. Y. Yao, Opt. Eng. **48**, 104302 (2009).
11. J. Vasseur, M. Hanna, J. M. Dudley, and J.-P. Goedgebuer, Electron. Lett. **40**, 901 (2004).
12. K. Lee, C. Shu, and H. F. Liu, IEEE J. Quantum Electron. **40**, 205 (2004).
13. K. L. Lee, M. P. Fok, and C. Shu, Opt. Commun. **251**, 149 (2005).
14. A. Zhang, J. Yu, L. Zhang, W. Wang, H. Hu, B. Han, Y. Jiang, and E. Yang, Proc. SPIE **7136**, 71362O (2008).
15. N. T. Hung, N.-T. Quang, M. Matsuura, and N. Kishi, J. Lightwave Technol. **30**, 853 (2012).
16. H. Q. Lam, K. E. K. Lee, and P. H. Lim, Opt. Lett. **37**, 2349 (2012).
17. D. Sinefeld, Y. Fattal, and D. M. Marom, Opt. Lett. **37**, 4290 (2012).
18. D. Sinefeld, S. Ben-Ezra, C. R. Doerr, and D. M. Marom, Opt. Lett. **36**, 1410 (2011).
19. A. M. Weiner, Prog. Quantum Electron. **19**, 161 (1995).
20. A. M. Weiner, Rev. Sci. Instrum. **71**, 1929 (2000).
21. E. Frumker and Y. Silberberg, Opt. Lett. **32**, 1384 (2007).
22. D. Sinefeld, C. R. Doerr, and D. M. Marom, Opt. Express **19**, 14532 (2011).
23. X. Yi, L. Li, T. X. H. Huang, and R. A. Minasian, Opt. Lett. **37**, 608 (2012).
24. J. C. Vaughan, T. Feurer, K. W. Stone, and K. A. Nelson, Opt. Express **14**, 1314 (2006).
25. D. Sinefeld and D. M. Marom, J. Lightwave Technol. **29**, 69 (2011).
26. K. Seno, N. Ooba, K. Suzuki, T. Watanabe, K. Watanabe, and S. Mino, IEEE Photon. Technol. Lett. **21**, 1701 (2009).
27. T. Xia and H. Zheng, IEEE Trans. Ind. Electron. **54**, 1014 (2007).